Optimal Design of PV Systems Considering Levelized Cost of Energy and Power Density

Dongsen Sun
Department of Electrical and Computer Engineering
Temple University
Philadelphia, PA, USA
dongsen.sun@temple.edu

Xiaonan Lu
Department of Electrical and Computer Engineering
Temple University
Philadelphia, PA, USA
xiaonan.lu@temple.edu

Liang Du
Department of Electrical and Computer Engineering
Temple University
Philadelphia, PA, USA
ldu@temple.edu

Yue Cao
School of Electrical Engineering and Computer Science
Oregon State University
Corvallis, OR, USA
yue.cao@oregonstate.edu

***Abstract*—This paper presents an optimal design framework for photovoltaic (PV) power generation systems. With the objectives of minimizing levelized cost of energy (LCOE) and maximizing power density (PD) of PV inverters, all design components of PV inverters including inverter topologies, semiconductor (SC) devices, DC bus capacitors, switching frequency, AC output filter, and cooling system are designed in a holistic framework. Particularly, the design framework is formulated as a constrained optimization problem to determine the optimal combination of key components of PV inverters. With real solar profiles, three 100-kW PV systems are designed featuring an optimal LCOE with different weather conditions, and a high PD and energy conversion efficiency can be guaranteed using the proposed framework. The testing results using field data demonstrate the effectiveness of the proposed optimal design framework.**

***Index Terms*—LCOE, optimal design, PV systems, power density, power loss**

I. Introduction

Motivated by increasing solar energy penetration and reducing the cost of PV power generation, there are tremendous efforts of PV power systems at residential, commercial, and utility levels. In order to enhance the performance of PV systems in both technical and financial aspects, it is necessary to investigate and develop an optimal design framework of PV systems. Various objectives are considered to optimize the design of PV systems. For instance, Ref. [1] designs the type of PV panel, the type of PV inverter, and the number of PV panels to maximize the financial benefits. However, PV inverter optimal design is not considered, and only commercially available PV inverters are considered.

As the backbone of PV power systems, PV inverters play a critical role in interfacing PV panels and external grids. The cost and volume of PV inverter also accounted for a considerable portion of the whole PV system; therefore, the optimal design of a PV inverter has a significant impact on the whole PV system's performance. Tremendous research efforts have been made to improve the efficiency, power quality, reliability, as well as to reduce the weight, volume, and cost of PV inverters over the past few years [2]–[7]. Different inverter topologies and semiconductor (SC) devices are investigated to improve the power density (PD) of the PV inverter in [2]–[4]. While in [5], [6], PV inverter reliability is included in the objectives of the optimal design of the whole system. In [7], two PV inverter topologies, H5 and Conergy-NPC, are investigated and the switching frequency and AC output filter are optimized to achieve a reduced levelized cost of energy (LCOE) [8], [9]. However, some other important PV inverter components, such as SCs, DC-link capacitors, and cooling systems, are not selected to be decision variables. A novel virtual prototyping routine for PV inverter design is investigated and a multi-objective optimization design considering inverter efficiency, PD, and the cost is detailed in [4]. However, this paper does not specifically consider the impacts of solar profiles at different locations. Due to different solar power availability and some cost-driven constraints, the location of the solar power generation site may lead to different optimal designs.

This paper proposes an optimal design framework for PV systems, which has a decision variable set including inverter topologies, SC devices, switching frequency, DC bus capacitors, output filters, and cooling systems. Additionally, two objectives, LCOE of the whole PV system and the PD of the PV inverter, are incorporated into the optimal design framework. Firstly, using the mathematical model of the whole PV system, the PV system design framework is formulated as a constrained optimization problem. Then, a heuristic algorithm, i.e., genetic algorithm (GA), is used to solve the optimization problem and to obtain the value of decision variables that satisfy the optimization objective. Three 100-kW PV systems in different installation sites are designed and studied, and the comparative study and the corresponding results demonstrate the effectiveness of the proposed optimal design framework.

II. PV System Component modeling

A typical PV system is shown in Fig. 1, which mainly consists of PV panels, DC bus capacitors, PV inverter, output filter, and utility grid or local load. The mathematical model of these components, including the physical and cost models, are presented in this section.

A. PV Panels

PV panels provide the electric energy to a utility grid or local users. Energy harvested by PV panels highly depends on

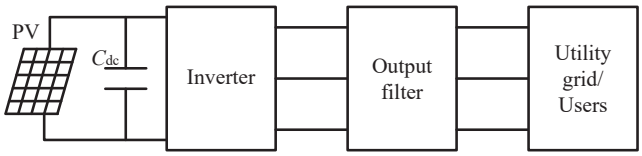

Fig. 1. Configuration of PV power generation system.

the weather condition (i.e., solar irradiation and temperature) at the installation site. Additionally, the energy produced by PV panels decrease every year during its lifetime as the PV panels degrade. The energy yield of PV panels in its lifetime year can be obtained as [9]

$$e_n = \begin{cases} 0 & n = 0 \\ \max[Y(1-R_d)^{n-1}, 0] & n > 0 \end{cases} \quad (1)$$

where Y is the first year energy yield and R_d is the PV system's annual degradation rate.

The cost of PV panels can be obtained from PV manufacturers or vendors.

B. DC Bus Capacitors

Due to the limited availability of the voltage and capacity rating of commercial capacitors, usually, several capacitors are connected in series and/or parallel to meet the design requirments. DC bus capacitors are used to limit DC voltage ripples and support DC bus voltage when there are voltage or power variations on the DC side.

DC bus capacitors' power loss is neglected due to its little impact on the total power loss. The cost and volume of the DC bus capacitors can be obtained from corresponding distributors.

C. PV Inverter

PV inverters are categorized into two-level and multi-level inverters based on the output voltage levels. There are a large number of multilevel PV inverter topologies, such as CHB, NPC, Active NPC, H4, H5, Conergy-NPC, and etc. [4], [7], [10]. However, as an example, only two topologies, traditional two-level and three-level NPC inverters shown in Fig. 2, are considered to be the PV inverter candidates in this paper.

Semiconductors are the main components of a PV inverter. An accurate power loss model of semiconductors is significant to the whole system optimization design because the power loss determines the efficiency, volume, and cost of the whole PV system. Power loss models of the two types of PV inverter topology are presented as follows, respectively.

1) Power loss model of two-level inverter: The semiconductor power loss of a two-level inverter includes conduction and switching loss of IGBTs and their free-wheeling diodes, which can be expressed as [11], [12]

$$P_{\text{SC2L}} = P_{\text{cond\_S2L}} + P_{\text{sw\_S2L}} + P_{\text{cond\_D2L}} + P_{\text{sw\_D2L}} \quad (2)$$

where $P_{\text{cond\_S2L}}$ and $P_{\text{sw\_S2L}}$ represent the conduction and switching loss of all IGBTs in a two-level inverter; $P_{\text{cond\_D2L}}$ and $P_{\text{sw\_D2L}}$ are the conduction and switching loss of all free-wheeling diodes, respectively.

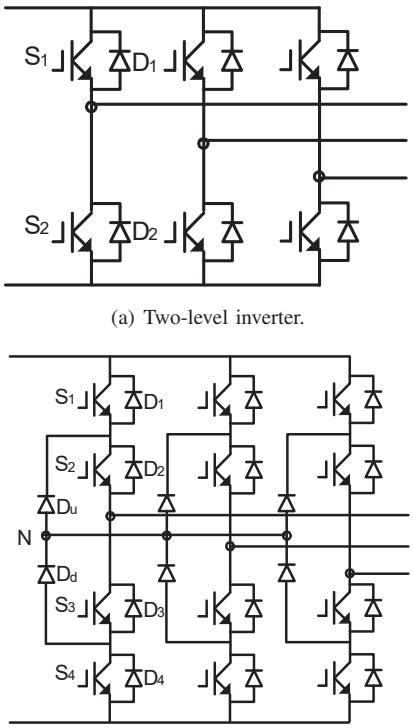

(a) Two-level inverter.

(b) Three-level inverter.

Fig. 2. Two-level and three-level PV inverter topology.

IGBTs conduction loss is calculated as:

$$P_{\text{cond\_S2L}} = N_{\text{S}}(u_{\text{ce0}} I_{\text{S,avg}} + r_S I^2_{\text{S,rms}}) \quad (3)$$

$$I_{\text{S,avg}} = (\frac{1}{2\pi} + \frac{M\cos\varphi}{8})I \quad (4)$$

$$I^2_{\text{S,rms}} = (\frac{1}{8} + \frac{M\cos\varphi}{3\pi})I^2 \quad (5)$$

where u_{ce0}, r_{S}, $I_{\text{S,avg}}$ and $I_{\text{S,rms}}$ are the IGBT on-state voltage drop, on-state resistance, average conduction current, and rms conduction current, respectively; N_{S} is the number of IGBT to calculate power loss; M is the modulation index that depends on the control and modulation scheme; I is the magnitude of the inverter output current; φ is the phase lagged by the inverter output current compared with the fundamental voltage of the inverter output voltage.

Diodes conduction loss is calculated as:

$$P_{\text{cond\_D2L}} = N_{\text{D}}(u_{\text{D0}} I_{\text{D,avg}} + r_{\text{D}} I^2_{\text{D,rms}}) \quad (6)$$

$$I_{\text{D,avg}} = (\frac{1}{2\pi} - \frac{M\cos\varphi}{8})I \quad (7)$$

$$I^2_{\text{D,rms}} = (\frac{1}{8} - \frac{M\cos\varphi}{3\pi})I^2 \quad (8)$$

where N_{D} is the number of diodes to calculate power loss; u_{D0}, r_{D}, $I_{\text{D,avg}}$ and $I_{\text{D,rms}}$ are diode on-state voltage drop, on-state

resistance, average conduction current, and rms conduction current, respectively.

IGBTs switching loss is:

$$P_{\text{sw\_S2L}} = N_{\text{S}} \frac{V_{\text{DD}} I_{\text{S,equ}}}{V_{\text{t}} I_{\text{t}}} (E_{\text{on\_S}} + E_{\text{off\_S}}) f_{\text{s}} \tag{9}$$

$$I_{\text{S,equ}} = \frac{I}{\pi} \tag{10}$$

where $E_{\text{on\_S}}$ and $E_{\text{off\_S}}$ are the turn on and off energy of IGBT under a certain test condition, respectively; V_{t} and I_{t} are the test voltage and current given in the data sheet of the device; V_{DD} is the voltage stress on the IGBT at the switching instant; $I_{\text{S,equ}}$ is the equivalent current of IGBT during a switching instant to calculate the switching loss; f_{s} is switching frequency.

Diodes switching loss is:

$$P_{\text{sw\_D2L}} = N_{\text{D}} \frac{V_{\text{DD}} I_{\text{D,equ}}}{V_{\text{t}} I_{\text{t}}} E_{\text{rec\_D}} f_{\text{s}} \tag{11}$$

$$I_{\text{D,equ}} = \frac{I}{\pi} \tag{12}$$

where $E_{\text{rec\_D}}$ is the reverse recovery energy of diode under a certain test condition; $I_{\text{D,equ}}$ is the equivalent current of the diode during a switching instant to calculate the switching loss.

2) Power loss model of three-level inverter: The power loss model of a three-level inverter not only includes the power loss of IGBTs and their free-wheeling diodes but also the power loss induced by additional clamped diodes. It can be expressed as [10], [13], [14]

$$\begin{aligned} P_{\text{SC3L}} = {} & P_{\text{cond\_S3L}} + P_{\text{sw\_S3L}} + P_{\text{cond\_D3L}} + P_{\text{sw\_D3L}} \\ & + P_{\text{cond\_CD}} + P_{\text{sw\_CD}} \end{aligned} \tag{13}$$

where $P_{\text{cond\_S3L}}$ and $P_{\text{sw\_S3L}}$ represent the conduction and switching loss of IGBTs in a three-level inverter; $P_{\text{cond\_D3L}}$ and $P_{\text{sw\_D3L}}$ are the conduction and switching loss of their free-wheeling diodes, respectively. $P_{\text{cond\_CD}}$ and $P_{\text{sw\_CD}}$ represent the conduction and switching loss of clamped diodes, respectively.

Power loss calculation of a three-level inverter is similar as that of a two-level inverter, thus the power loss calculation equations will not be repeated here. Instead, only the average, rms and equivalent current of the semiconductor devices are presented. Additionally, as the symmetric operation of the devices in a three-level inverter, only the currents of four devices, S_1, S_2, D_1, D_u, are listed and other devices' currents can be obtained accordingly.

$$I_{\text{S}_1\text{,avg}} = \frac{M(\sin\varphi + \pi\cos\varphi - \varphi\cos\varphi)}{4\pi} I \tag{14}$$

$$I^2_{\text{S}_1\text{,rms}} = \frac{M(\cos\varphi + 1)^2}{6\pi} I^2 \tag{15}$$

$$I_{\text{S}_1\text{,equ}} = \frac{\cos\varphi + 1}{2\pi} I \tag{16}$$

$$I_{\text{S}_2\text{,avg}} = (\frac{1}{\pi} - \frac{M\sin\varphi}{4\pi} + \frac{M\varphi\cos\varphi}{4\pi}) I \tag{17}$$

$$I^2_{\text{S}_2\text{,rms}} = (\frac{1}{4} - \frac{M(\cos\varphi - 1)^2}{6\pi}) I^2 \tag{18}$$

$$I_{\text{S}_2\text{,equ}} = \frac{1 - \cos\varphi}{2\pi} I \tag{19}$$

$$I_{\text{D}_1\text{,avg}} = (\frac{M\sin\varphi}{4\pi} - \frac{M\varphi\cos\varphi}{4\pi}) I \tag{20}$$

$$I^2_{\text{D}_1\text{,rms}} = \frac{M(\cos\varphi - 1)^2}{6\pi} I^2 \tag{21}$$

$$I_{\text{D}_1\text{,equ}} = \frac{1 - \cos\varphi}{2\pi} I \tag{22}$$

$$I_{\text{D}_u\text{,avg}} = (\frac{1}{\pi} - \frac{M(\sin\varphi - \varphi\cos\varphi)}{2\pi} - \frac{M\pi\cos\varphi}{4\pi}) I \tag{23}$$

$$I^2_{\text{D}_u\text{,rms}} = (\frac{1}{4} - \frac{M(\cos^2\varphi + 1)}{3\pi}) I^2 \tag{24}$$

$$I_{\text{D}_u\text{,equ}} = \frac{I}{\pi} \tag{25}$$

Semiconductors' cost and volume can be obtained from the corresponding manufacturers or distributors.

D. Output Filter

To meet the power quality requirement of utility gird or users, AC filters are always installed at the output side of PV inverters to eliminate the harmonics. Here an LCL-filter is employed for the designed PV system.

An LCL-filter is compromised of an inverter-side inductor, a filter capacitor, and a grid-side inductor. Neglecting the power loss of the filter capacitor, the power loss of an LCL-filter can be calculated by

$$P_{\text{LCL}} = P_{\text{li}} + P_{\text{lg}} \tag{26}$$

where P_{li} and P_{lg} are the power loss of the inverter-side and grid-side inductors, respectively.

The cost and volume of an LCL-filter can be obtained by summing up the cost and volume of the inverter-side inductor, filter capacitor, and gird-side inductor, respectively. Detailed price information and specification of the LCL-filter can be obtained from the corresponding manufacturers or distributors.

E. Cooling System

The cooling system helps dissipate the heat generated by all the components, especially the heat generated by semiconductor devices. Typically, a cooling system consists of two parts, i.e., heat sink and fan. A desirable cooling system should feature a lower thermal resistance, which is determined by the type and size of the heat sink as well as the flow velocity of the fan.

Taking an Aavid product (Extrusion 64360) as an example, its thermal performance with different size of the heat sink and different velocities of the fan is shown in Fig. 3 [15]. The thermal resistance is decreasing with the increase of the heat sink's length and the fan's flow velocity.

The cost and volume of the whole cooling system can be obtained by summing up the cost and volume of the fan and

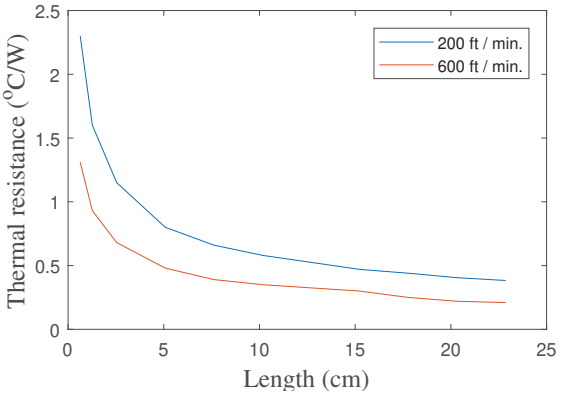

Fig. 3. Characteristic of a cooling system.

heat sink, respectively. The detailed price and specification of the cooling system can be obtained from corresponding manufactures or their vendors.

III. Formulation of the Optimal Design of PV Systems

The formulation of this design problem is shown in this section, which includes decision variables, objectives, and all constraints. The flow chart of the whole optimization process is shown in Fig. 4. Initially, solar power data, system specifications, decision variables, and all constraints are defined according to the designer's demand. Then a set of the feasible combinations of decision variables is generated. With the component models derived in Section II, the value of the weighted objective function is obtained. Finally, GA is used to solve the problem, and the optimizer and the optimal decision variables are obtained.

A. Decision Variables

Decision variables are selected per the actual operational requirements to achieve an optimal design of the PV system. Here, the decision variables are

$$\mathbf{X} = [\sigma_{\text{TP}}\ \sigma_{\text{SC}}\ \sigma_{\text{CS}}\ f_{\text{s}}\ L_{\text{i}}\ C_{\text{f}}\ L_{\text{g}}\ C_{\text{dc}}] \tag{27}$$

where $\sigma_{\text{TP}}, \sigma_{\text{SC}}, \sigma_{\text{CS}}, f_{\text{s}}, L_{\text{i}}, C_{\text{f}}, L_{\text{g}}$, and C_{dc} represent inverter topology, SC device, cooling system, switching frequency, inverter-side inductor, filter capacitor, grid-side inductor, and DC bus capacitor, respectively.

In our design only two inverter topologies, i.e., two-level VSI and three-level NPC are considered, so σ_{TP} will be one of the two candidates. And it can be expressed as

$$\sigma_{\text{TP}} = \begin{cases} 1, & \text{if two-level topology is selected} \\ 0, & \text{if three-level topology is selected} \end{cases} \tag{28}$$

Based on the capacity of the PV inverter, a number of commercially available semiconductor devices are pre-selected to be candidates for the optimization design. σ_{SC} will be a semiconductor device selected from the list. In this design, the thermal resistance is used to characterize the performance of a cooling system. With the obtained thermal resistance, a cooling system with specific heat sink and fan can be selected.

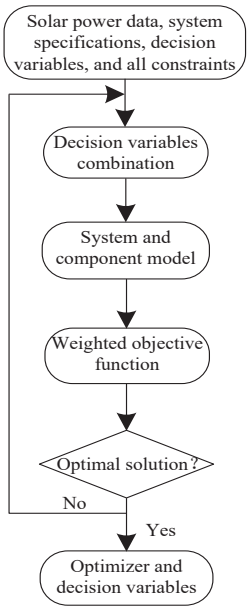

Fig. 4. Flow chart of the proposed optimization design method.

B. Objective Function

Design objectives are to minimize the LCOE of the PV system and to maximize the PD of PV inverter. These two objectives can be weighted and expressed as

$$F(\mathbf{X}) = \alpha LCOE(\mathbf{X}) + \beta PD(\mathbf{X}) \tag{29}$$

where $LCOE$ is the levelized cost of energy of the PV system; PD is the power density of the PV inverter; α and β are weighted coefficients, which are determined according to designers' preference.

1) LCOE: [9]

$$LCOE(\mathbf{X}) = C_{\text{total}}(\mathbf{X})/E_{\text{total}}(\mathbf{X}) \tag{30}$$

where C_{total} is the total cost of the PV system including initial investment and the operation and maintenance (O&M) cost. E_{total} is the total energy injected into utility grid or users end during the PV system service lifetime.

C_{total} can be calculated by

$$C_{\text{total}}(\mathbf{X}) = C_{\text{PV}} + C_{\text{inv}}(\mathbf{X}) + C_{\text{BOS}}(\mathbf{X}) + N_{\text{lf}} C_{\text{O\&M}}(\mathbf{X}) \tag{31}$$

where C_{PV} and C_{inv} are the cost of PV panels and PV inverter, respectively. C_{BOS} is the cost of the balance of system (BOS), which includes the the power-scaling (without inverter cost) and area-scaling BOS cost; N_{lf} is the PV system service lifetime; and $C_{\text{O\&M}}$ is the annual O&M cost of the PV system.

Inverter cost is expressed as

$$C_{\text{inv}}(\mathbf{X}) = C_{\text{SC}}(\mathbf{X}) + C_{\text{CS}}(\mathbf{X}) + C_{\text{LCL}}(\mathbf{X}) + C_{\text{Cdc}}(\mathbf{X}) + C_{\text{AUX}} \tag{32}$$

where C_{SC}, C_{CS}, C_{LCL}, C_{Cdc}, C_{AUX} are the cost of semiconductors, cooling system, LCL-filter, DC bus capacitor, and

auxiliary components, respectively. Note that the auxiliary components cost can be expressed as a fixed cost, which includes the cost of gate drivers, control unit, voltage and current transducers, all PCBs, and all accessory components such as wires, breakers, etc..

E_{total} can be obtained by

$$E_{\text{total}}(\mathbf{X}) = \sum_{n=1}^{N_{\text{lf}}} e_n \tag{33}$$

2) Power density:

The power injected into electric grid can be obtained by

$$P_{\text{g}}(\mathbf{X}) = P_{\text{in}}(\mathbf{X}) - P_{\text{loss}}(\mathbf{X}) \tag{34}$$

where P_{in} is the input power of PV inverter and P_{loss} is the total power loss of PV inverter.

Power density of the PV inverter is obtained as

$$PD(\mathbf{X}) = P_{\text{r}}(\mathbf{X})/V_{\text{vol}}(\mathbf{X}) \tag{35}$$

where P_r is the power rating of PV inverter, and V_{vol} is the total volume of components of the PV inverter.

V_{vol} can be calculated by

$$V_{\text{vol}}(\mathbf{X}) = V_{\text{SC}}(\mathbf{X}) + V_{\text{CS}}(\mathbf{X}) + V_{\text{LCL}}(\mathbf{X}) + V_{\text{Cdc}}(\mathbf{X}) \tag{36}$$

where V_{SC}, V_{CS}, V_{LCL}, V_{Cdc} are the volume of the semiconductors, cooling system, LCL-filter, and DC bus capacitors, respectively. Here, the volume of auxiliary components has been neglected due to their little impact on the total volume.

C. Constraints

The junction temperature of each SC chip in an SC device cannot be higher than its maximum temperature specified in its datasheet. Thus, thermal limits of all SC chips are [16]

$$\begin{aligned} T_{\text{j},i}(\mathbf{X}) &= R_{\text{j-c},i}(\mathbf{X}) P_{\text{SC},i}(\mathbf{X}) + \sum_{i=1}^{N_{\text{ch}}} R_{\text{c-h},i}(\mathbf{X}) P_{\text{SC},i}(\mathbf{X}) \\ &\quad + R_{\text{CS}}(\mathbf{X}) \sum_{i=1}^{N_{\text{ch}}} P_{\text{SC},i}(\mathbf{X}) + T_{\text{amb}} \\ &\quad \leq T_{\text{jmax},i}(\mathbf{X}) \end{aligned} \tag{37}$$

where $T_{\text{j},i}$, $R_{\text{j-c},i}$, $P_{\text{SC},i}$, and $T_{\text{jmax},i}$ are the junction temperature, the junction to case thermal resistance, the power loss, and the maximum junction temperature of the ith SC chip in a SC device, respectively. T_{amb} is the ambient temperature, N_{ch} is the number of chip consisted in a SC device, and R_{CS} is the thermal resistance of the cooling system.

To avoid excessive voltage drop on the output filter inductors, the sum of L_{i} and L_{g} is limited to be [7], [17]

$$L_{\text{i}} + L_{\text{g}} \leq 0.1 L_{\text{b}} \tag{38}$$

where L_{b} is the inductance base, which can be calculated based on the specification of PV inverter.

The most important feature of a LCL-filter is the resonance frequency, which determines the performance of the filter. It can be calculated by

$$f_{\text{res}}(\mathbf{X}) = \sqrt{\frac{L_{\text{i}} + L_{\text{g}}}{L_{\text{i}} L_{\text{g}} C_{\text{f}}}} \tag{39}$$

To avoid instability issues, the resonance frequency of the LCL-filter should be set as [7], [17]:

$$10f \leq f_{\text{res}}(\mathbf{X}) \leq f_{\text{sm}}/2 \tag{40}$$

where f is the fundamental frequency, and f_{sm} is the sampling frequency.

To limit the reactive power flow in the filter capacitor, the filter capacitance should meet

$$C_{\text{f}} \leq 5\% C_{\text{b}} \tag{41}$$

where C_{b} is the capacitance base and it can be calculated based on the specification of the PV inverter.

DC bus capacitance should meet the following inequality to mitigate voltage ripples at the DC side [17]

$$C_{\text{dc}} \geq \frac{T_{\text{r}} \Delta P}{2 \Delta V_{\text{dc}} V_{\text{dc}}} \tag{42}$$

where T_{r} is the time delay introduced by control unit, ΔP is the power variation, V_{dc} is the DC bus voltage, and ΔV_{dc} is the voltage variation of V_{dc}.

The efficiency of the PV inverter can be calculated by

$$\eta(\mathbf{X}) = \frac{P_{\text{g}}(\mathbf{X})}{P_{\text{in}}(\mathbf{X})} \tag{43}$$

PV inverter efficiency should be no less than an expected value, which is

$$\eta(\mathbf{X}) \geq \eta_{\text{min}} \tag{44}$$

where η_{min} is the minimum efficiency requirement of the PV inverter.

Finally, the size of heat sinks should fit SC devices.

IV. Case Study

To demonstrate the optimal design framework, three PV systems in Texas (TX), Pennsylvania (PA), and Minnesota (MN) are designed and tested. Solar power data at each location is downloaded from National Renewable Energy Lab (NREL) website [18] to calculate the energy production of PV panels. Fig. 5 shows a year of solar power profiles of TX, PA, and MN, respectively. From the figure, we can observe that the PV panels installed in TX can harvest more energy than the other two locations. Other specifications and parameters of the PV systems are listed as follows: power rating of the PV inverters is 100 kW; utility grid is 480 V/60 Hz; DC bus voltage is 1200 V; the minimum PV inverter efficiency is 98%; the service lifetime of the designed PV systems is 30 years, and the energy harvesting degradation rate is 0.36%; there are two candidate inverter topologies, two-level and three-level NPC; two SC devices are provided for each inverter topology, i.e., FF200R17KE4 and FF225R17ME4 for two-level inverters, and FF200R12KE4 and FF225R12ME4 for

TABLE I
OPTIMIZATION RESULTS OF THREE PV SYSTEMS IN DIFFERENT INSTALLATION SITES

Site	σ_{TP}	σ_{SC}	$\sigma_{CS}(^oC/W)$ R_{igbt}	R_{CD}	f_s (Hz)	L_i (μH)	C_f (μF)	L_g (μH)	C_{dc} (μF)	$LCOE$ $(\$/kW)$	PD (kW/dm^3)	F	η (%)
TX	0	2^{nd}	0.57	0.67	6200	88.0	57.6	95.4	278	0.07	3.49	1.82	98.3
PA	0	2^{nd}	0.57	0.67	6200	91.6	57.6	91.6	278	0.08	3.49	2.32	98.3
MN	0	2^{nd}	0.57	066	6300	90.1	57.6	87.4	278	0.1	3.50	3.39	98.3

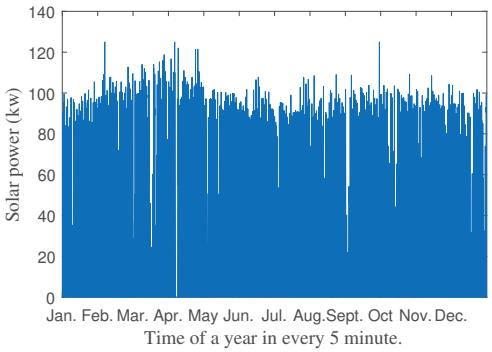

(a) Solar profile of a year in TX.

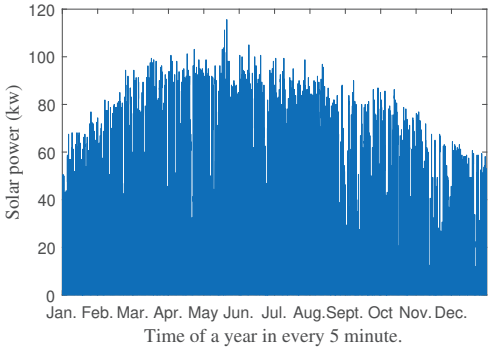

(b) Solar profile of a year in PA.

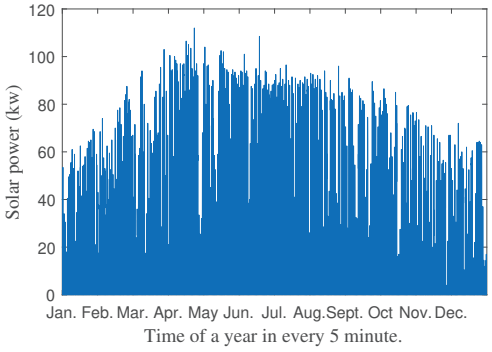

(c) Solar profile of a year in MN.

Fig. 5. Solar profile in different locations.

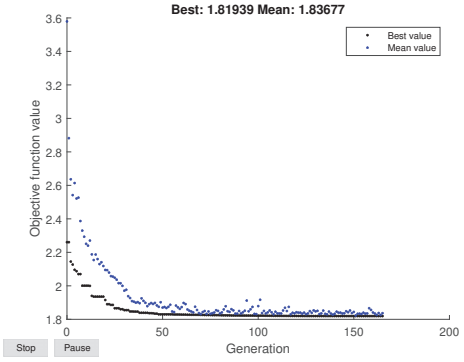

(a) The optimization result of the PV system in TX.

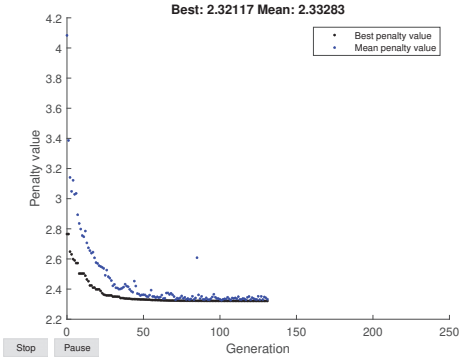

(b) The optimization result of the PV system in PA.

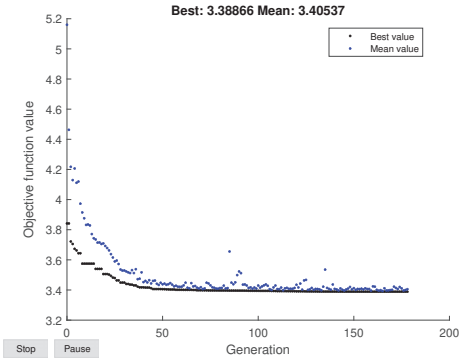

(c) The optimization result of the PV system in MN.

Fig. 6. GA optimization results of the PV systems.

three-level inverters; CD61 is used for the clamped diodes of three-level inverter; cooling system is comprised of a fan with a given flow velocity of 200 ft/min and a heat sink of Aavid product with part no. of 64360 [15]; note that the types of semiconductor device and heat sink are limited in the example case, actually more options can be added according to the demand in the practical design cases; weighted coefficients are set to $\alpha = \beta = 0.5$.

GA is used for three cases and the optimization procedures of three cases are shown in Fig. 6. As shown in Fig. 6, the

objective function reaches the minimum value of 1.82, 2.32, and 3.39, respectively. Table I shows the final design of PV inverter at each location, where the values of all decision variables in the three cases are detailed. As shown in Table I, three-level inverter topology and the second type of the SC device are selected to achieve the optimal results in all three cases. Meanwhile, other decision variables, i.e. thermal resistance of the cooling system, switching frequency, LCL filter parameters, DC bus capacitance are also shown in Table I. From Table I, it is observed that with different switching frequencies, three PV systems have different inductance and capacitance in the LCL-filters and different thermal resistance in the cooling systems.

The detailed design of three PV systems are also shown in Table I. LCOE of the cases in TX, PA, and MN are \$0.07, \$0.08, and \$0.1, respectively. With the best weather condition, PV systems installed in TX can capture more solar energy than the other two sites. Therefore, the PV system installed in TX can achieve the lowest LCOE even with the same initial investment and O&M cost as those of the other two sites. Another objective, PD of PV inverter, is also used to evaluate the performance of the PV systems. As shown in Table I, all three PV systems show very good performance with the proposed design method. The PD and efficiency of all the three PV inverters are around 3.5 kW/dm^3 and 98.3%.

V. Conclusion

This paper proposed an effective optimal design framework for PV power generation systems. A suitable set of decision variables is considered compared to the existing work, and the optimization problem can be solved efficiently with GA-based solver. Field solar profiles and component costs from distributors or vendors are used to design the three PV systems installed in TX, PA, and MN. Optimization results validate that the proposed optimal design framework can be used to design PV systems at different installation sites and the designed PV system can guarantee an expected performance.

References

[1] S. A. Arefifar, F. Paz, and M. Ordonez, "Improving solar power pv plants using multivariate design optimization," *IEEE Journal of Emerging and Selected Topics in Power Electronics*, vol. 5, no. 2, pp. 638–650, 2017.

[2] Y. Shi, L. Wang, R. Xie, and H. Li, "Design and implementation of a 100 kw sic filter-less pv inverter with 5 kw/kg power density and 99.2% cec efficiency," in *2018 IEEE Applied Power Electronics Conference and Exposition (APEC)*. IEEE, 2018, pp. 393–398.

[3] C. Zhang, S. Srdic, S. Lukic, Y. Kang, E. Choi, and E. Tafti, "A sic-based 100 kw high-power-density (34 kw/l) electric vehicle traction inverter," in *2018 IEEE Energy Conversion Congress and Exposition (ECCE)*. IEEE, 2018, pp. 3880–3885.

[4] R. M. Burkart and J. W. Kolar, "Comparative life cycle cost analysis of Si and SiC pv converter systems based on advanced $\eta - \rho - \sigma$ multiobjective optimization techniques," *IEEE Transactions on power electronics*, vol. 32, no. 6, pp. 4344–4358, 2017.

[5] E. Koutroulis and F. Blaabjerg, "Design optimization of transformerless grid-connected pv inverters including reliability," *IEEE Transactions on Power Electronics*, vol. 28, no. 1, pp. 325–335, 2013.

[6] T. Dragicevic, P. Wheeler, and F. Blaabjerg, "Artificial intelligence aided automated design for reliability of power electronic systems," *IEEE Transactions on Power Electronics*, 2018.

[7] S. Saridakis, E. Koutroulis, and F. Blaabjerg, "Optimization of sic-based H5 and Conergy-NPC transformerless pv inverters," *IEEE Journal of Emerging and Selected Topics in Power Electronics*, vol. 3, no. 2, pp. 555–567, 2015.

[8] R. Fu, D. Feldman, and R. Margolis, "U.S. solar photovoltaic system cost benchmark: Q1 2018," National Renewable Energy Laboratory, Tech. Rep., 2018.

[9] T. Silverman, M. Deceglie, and K. Horowitz, "NREL comparative PV LCOE calculator," http://pvlcoe.nrel.gov, March 2018.

[10] S. Saridakis, E. Koutroulis, and F. Blaabjerg, "Optimal design of modern transformerless pv inverter topologies," *IEEE transactions on energy conversion*, vol. 28, no. 2, pp. 394–404, 2013.

[11] D. Graovac and M. Purschel, "Igbt power losses calculation using the data-sheet parameters,‖ infineon application note," 2009.

[12] J. W. Kolar, H. Ertl, and F. C. Zach, "Influence of the modulation method on the conduction and switching losses of a pwm converter system," *IEEE Transactions on Industry Applications*, vol. 27, no. 6, pp. 1063–1075, 1991.

[13] G. Kalcon, G. P. Adam, O. Anaya-Lara, G. Burt, and K. Lo, "Analytical efficiency evaluation of two and three level vsc-hvdc transmission links," *International Journal of Electrical Power & Energy Systems*, vol. 44, no. 1, pp. 1–6, 2013.

[14] K. A. Tehrani, I. Rasoanarivo, and F.-M. Sargos, "Power loss calculation in two different multilevel inverter models (2dm2)," *Electric Power Systems Research*, vol. 81, no. 2, pp. 297–307, 2011.

[15] "Data and performance of aavid product 64360," https://www.shopaavid.com/Product/64360-full.

[16] R. M. Burkart, "Advanced modeling and multi-objective optimization of power electronic converter systems," Ph.D. dissertation, ETH Zurich, 2016.

[17] L. Malesani, L. Rossetto, P. Tenti, and P. Tomasin, "AC/DC/AC pwm converter with reduced energy storage in the dc link," *IEEE Transactions on Industry Applications*, vol. 31, no. 2, pp. 287–292, 1995.

[18] "Solar power data for integration studies," https://www.nrel.gov/grid/solar-power-data.html.